THEORETICAL & APPLIED MECHANICS LETTERS **4**, 022001 (2014)

Unified gas-kinetic simulation of slider air bearing

Ruijie Wang,[1] Kun Xu[2, a)]

[1)]*Department of Fluid Mechanics, School of Aeronautics, Northwestern Polytechnical University, Xi'an 710072, China*

[2)]*Department of Mathematics, School of Science, Hong Kong University of Science and Technology, Hong Kong, China*

(Received 17 January 2014; accepted 20 January 2014)

Abstract The unified gas-kinetic scheme (UGKS) is presented and used in this letter to study the slider air bearing problem. The UGKS solutions are first validated by comparison with direct simulation Monte Carlo results. After validation, the UGKS is used to study the air-bearing problem under different non-equilibrium conditions. On the surface of the slider, the dependency of the gas pressure and normal force on the Mach and Knudsen numbers are fully evaluated. The non-equilibrium effect on the force loading in the whole transition regime up to the free molecular limit is also studied.

 [doi:10.1063/2.1402201]

Keywords unified gas-kinetic scheme, slider air-bearing, non-equilibrium

The slider air bearing problem arises from the hard disk industry. The demand of higher recording density requires the spacing between the read/write head and the disk to be on the nano scale, where the gas is rarefied and non-equilibrium phenomena may occur. New technologies have also been developed over the years to further increase the recording density, such as the heat-assisting magnetic recording (HAMR) that introduces a heat source into the slider system. Both the nano-scale flying height of the slider and the heat source could affect the bearing force on the slider, which is considered crucial in the slider design.

Due to the rarefaction of the gases in the slider air bearing problem, methods based on the kinetic theory should be employed instead of hydrodynamic equations. One successful method is the molecular gas-film lubrication (MGL) equation developed by Fukui and Kaneko,[1] which is basically the Reynolds equation corrected by the linearized Boltzmann equation. Efforts are also devoted to further extend the MGL equation to HAMR system by considering the thermal creep.[2] The direct simulation Monte Carlo (DSMC) method is well established and verified for the simulation of rarefied gases. The DSMC method was utilized by Alexander et al.[3] to study the slider air bearing problem in two-dimensions, and the non-equilibrium effect due to the increase of Mach number was discussed. Huang et al.[4] performed a three-dimensional simulation with DSMC and compared the bearing force with MGL. Myo et al.[5–7] studied the bearing characteristics on both patterned media and HAMR system by DSMC, discussed the influence of different geometric and physical parameters.

In this letter, the unified gas-kinetic scheme (UGKS)[8–10] is used to perform the numerical simulations. The method will be briefly described in the following part. The UGKS will be

[a)]Corresponding author. Email: makxu@ust.hk.

validated by comparing its results with the DSMC solutions of Alexander et al.[3] and Myo et al.,[6] where in the latter case a heat spot is introduced on the disk. The normal force on the slider, calculated from the non-equilibrium momentum transport, deviates from the gas pressure at high Mach and Knudsen numbers.[3] The details of force versus gas pressure as functions of Mach and Knudsen numbers will be presented and analyzed.

The UGKS is a multi-scale method based on the kinetic equation for simulating flows of all Knudsen numbers.[8–10] This part is a brief description of the method.

The kinetic equation without external force is

$$\frac{\partial f}{\partial t}+u_i\frac{\partial f}{\partial x_i}=Q,\ i=1,2,3, \tag{1}$$

where $f=f(x_i,t,u_i)$ represents the particle velocity distribution function at location x_i, time t, and particle velocity u_i, and Q is the collision term. Based on Eq. (1), the evolution of the distribution function under the framework of finite volume method is

$$f^{n+1}=f^n-\frac{1}{\Omega}\sum_m \mathscr{F}_m+\int_{t^n}^{t^{n+1}} Q\,\mathrm{d}t \tag{2}$$

and the evolution of mass, momentum, and energy densities, i.e., $\boldsymbol{W}$ is

$$\boldsymbol{W}^{n+1}=\boldsymbol{W}^n-\frac{1}{\Omega}\sum_m \boldsymbol{F}_m, \tag{3}$$

where Ω is the volume of the cell, m is the number of interfaces of the cell, $\mathscr{F}$ and $\boldsymbol{F}$ are the transports of f and $\boldsymbol{W}$ across the cell interface during a time step.

Construction of the interface flux is the core of UGKS. Suppose an interface is located at $\boldsymbol{x}=\boldsymbol{0}$ with unit outward normal $\boldsymbol{n}$ and area S, the distribution function at the interface from $t^n=0$ to $t^{n+1}=\Delta t$ is modeled by the solution of the Bhatnagar–Gross–Krook type (BGK-type) equation along the characteristic line as

$$f(\boldsymbol{0},t,\boldsymbol{u})=\frac{1}{\tau}\int_0^t g(\boldsymbol{x}',t',\boldsymbol{u})\mathrm{e}^{-(t-t')/\tau}\,\mathrm{d}t'+\mathrm{e}^{-t/\tau}f_0(-\boldsymbol{u}t,\boldsymbol{u}), \tag{4}$$

where $\boldsymbol{x}'=-\boldsymbol{u}(t-t')$, τ denotes the collision time, g represents the equilibrium distribution, and f_0 is the distribution function at $t^n=0$. The initial distribution function $f_0(\boldsymbol{x},\boldsymbol{u})$ is assumed to be linearly distributed within each cell and be discontinuous at the interface

$$f_0=(f_0^{\mathrm{L}}+x_i f_{x_i}^{\mathrm{L}})(1-H(\bar{x}))+(f_0^{\mathrm{R}}+x_i f_{x_i}^{\mathrm{R}})H(\bar{x}), \tag{5}$$

where $\bar{x}=x_i n_i$, f_0^{L}, f_0^{R} are the reconstructed distribution functions at the left side and right side of the cell interface, $f_{x_i}^{\mathrm{L}}$, $f_{x_i}^{\mathrm{R}}$ are the corresponding partial derivatives, and $H(x)$ is the Heaviside function

$$H(x)=\begin{cases}0, & x<0,\\ 1, & x\geqslant 0.\end{cases} \tag{6}$$

The equilibrium distribution function $g(\boldsymbol{x},t,\boldsymbol{u})$ is approximated by the first-order Taylor expansion of $g_0 = g(\mathbf{0},0,\boldsymbol{u})$, but has different normal partial derivatives across the interface and keeps the same constant along the interface for the directional splitting scheme

$$g = g_0[1 + (1 - H(\bar{x}))a^{\mathrm{L}}\bar{x} + H(\bar{x})a^{\mathrm{R}}\bar{x} + At]. \tag{7}$$

Here g_0 is uniquely determined by $\boldsymbol{W}_0 = \boldsymbol{W}(\mathbf{0},0)$

$$\boldsymbol{W}_0 = \int [f_0^{\mathrm{L}} H(\bar{u}) + f_0^{\mathrm{R}}(1 - H(\bar{u}))]\boldsymbol{\psi}\,\mathrm{d}u, \tag{8}$$

where $\bar{u} = u_i n_i$, $\mathrm{d}u = \mathrm{d}u_1\,\mathrm{d}u_2\,\mathrm{d}u_3$, and $\boldsymbol{\psi} = \{1, \boldsymbol{u}, u_i u_i/2\}^{\mathrm{T}}$ is the collisional invariants. The coefficients a^{L}, a^{R}, A are computed via the partial derivatives of conservative variables at $(\boldsymbol{x},t) = (\mathbf{0},0)$, for example

$$a^{\mathrm{L,R}} = \frac{1}{g_0}\left(\frac{\partial g_0}{\partial \boldsymbol{W}_0}\right)\boldsymbol{W}_{\bar{x}}^{\mathrm{L,R}} \approx \frac{1}{g_0}\left(\frac{\partial g_0}{\partial \boldsymbol{W}_0}\right)\frac{\boldsymbol{W}^{\mathrm{L,R}} - \boldsymbol{W}_0}{x_i^{\mathrm{L,R}} n_i}, \tag{9}$$

where $W^{\mathrm{L,R}}$ is the conservative variables at the left/right cell and $x_i^{\mathrm{L,R}}$ is the coordinate of the left/right cell center. The time derivative part A could be computed via,[11]

$$W_t = -\int [a^{\mathrm{L}} H(\bar{u}) + a^{\mathrm{R}}(1 - H(\bar{u}))]\bar{u} g_0 \boldsymbol{\psi}\,\mathrm{d}u. \tag{10}$$

The interface distribution function is completely determined by substituting Eqs. (5) and (7) into Eq. (4), and the interface flux transport of f and $\boldsymbol{W}$ during the whole time step are

$$\mathscr{F} = S\int_{t^n}^{t^{n+1}} \bar{u} f(\mathbf{0},t,\boldsymbol{u})\,\mathrm{d}t, \quad \boldsymbol{F} = \int \mathscr{F}\boldsymbol{\psi}\,\mathrm{d}u. \tag{11}$$

The conservative variables could be updated via Eq. (3) once the interface flux is known. And if the BGK collision term is adopted and the trapezoidal rule is applied to the collision term, Eq. (2) becomes

$$f^{n+1} = f^n - \frac{1}{\Omega}\sum_m \mathscr{F}_m + \frac{\Delta t}{2}(Q^n + Q^{n+1}), \tag{12}$$

where $Q = (g - f)/\tau$. Equation (2) is semi-implicit, but can be explicitly solved since $\boldsymbol{W}^{n+1}$ is known, from which g^{n+1} and τ^{n+1} are fully determined.

The UGKS method is a partial differential equation-based (PDE-based) modeling method instead of pure discretization of PDE. The core of UGKS is the use of a time evolution solution of BGK-type equation as shown in Eq. (4), and this solution covers different flow regimes. The time evolution solution presents a process from the free molecular flow to the Navier–Stokes solutions, and the solution used for the numerical flow evolution is determined by the ratio of the computational time step to the local particle collision time. Thus, different flow physics can be recovered under different conditions. For example, if the particle mean free path is larger than

the cell size, the free transport term in Eq. (4) will dominate and the kinetic scale flow physics is recovered. If the particle mean free path is much smaller than the cell size, the particle collision effect will dominate, and the Navier–Stokes distribution function can be obtained. Transition among different flow evolution mechanism can be achieved smoothly without using any switch function. The cell size and time step in UGKS are not limited to the particle mean free path and collision time, and the scheme can be used for all Knudsen numbers. In addition, the collision term used in the UGKS is not limited to BGK model, other relaxation model can be used as well.

In this paper, the BGK–Shakhov model is employed in the evaluation of both interface flux and collision term. The collision time is determined by the ratio of viscosity coefficient to pressure $\tau = \mu/p$. The viscosity is $\mu = \mu_{\text{ref}}(T/T_{\text{ref}})^{\omega}$, where μ_{ref} and T_{ref} are the reference viscosity and temperature, and ω is the temperature dependent index.

The schematic of the two-dimensional slider air bearing problem without heat spot is shown in Fig. 1. A stationary wall with length L_1 and temperature T_0 is inclined above a moving wall with velocity U, temperature T_0, and length L. Inlet and outlet are connected to the environment, where the ambient pressure and temperature are fixed at $p_0 = 1$ atm (1 atm = 101 325 Pa) and $T_0 = 273$ K. If the heat spot is introduced on the disk, the temperature distribution on the disk is no longer constant. Following Myo et al.,[6,7] the temperature distribution is assumed to be a sine wave with peak value 773 K, as shown in Fig. 2.

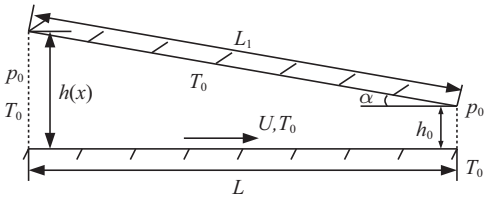

Fig. 1. Schematic of the slider air bearing without heat spot.

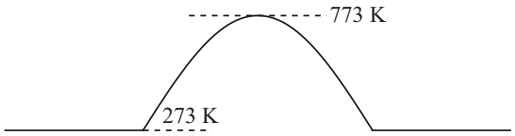

Fig. 2. Temperature distribution on disk with heat spot.

The pressure inlet/outlet boundary condition based on the characteristics of Euler equations is adopted to have a better comparison with the solution of MGL equation. And fully diffusive boundary conditions are used for both walls.

The system is characterised by the ratio of length to height L/h_0, the inclination angle α, the Mach number $Ma = U/\sqrt{\gamma RT_0}$, and the Knudsen number $Kn = \lambda/h_0$, where γ denotes the ratio of specific heat, R represents the gas constant, and λ is the mean free path.

The load w on the slider is defined as follows.[3] The pressure load is

$$w_p = \frac{1}{L}\int_0^L \frac{p(x) - p_0}{p_0}\,\mathrm{d}x, \tag{13}$$

where p is the pressure

$$p = \frac{1}{3}\int (\boldsymbol{u} - \boldsymbol{U})^2 f\,\mathrm{d}u, \tag{14}$$

and the force load is

$$w_f = \frac{1}{L}\int_0^L \frac{F(x) - p_0}{p_0}\,\mathrm{d}x, \tag{15}$$

where $F(x)$ is the distribution of normal force exerted on the slider per unit area. At each position of the slider, F is calculated via

$$F = \int (\boldsymbol{u}\cdot\boldsymbol{n})^2 f\,\mathrm{d}u, \tag{16}$$

in which f denotes the distribution function on the slider surface, $\boldsymbol{n}$ is the unit outward normal of the slider. The difference between w_p and w_f is an indication of non-equilibrium property of the flow. In the equilibrium case, the values of w_p and w_f should be the same due to the isotropic equilibrium state.

In order to validate UGKS, the simulation results are first compared with the DSMC solutions of Alexander et al.[3] in the following cases. The length/height ratio is $L/h_0 = 100$, and the inclination angle is $\alpha = 0.01$ rad. The gas is hard-sphere argon. Figures 3–5 show comparison of pressure distribution for cases with different Mach numbers and Knudsen numbers. Good agreement has been obtained in all cases.

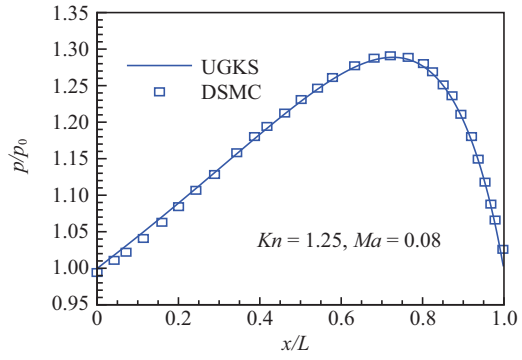

Fig. 3. Pressure distribution for $Kn = 1.25$ and $Ma = 0.08$.

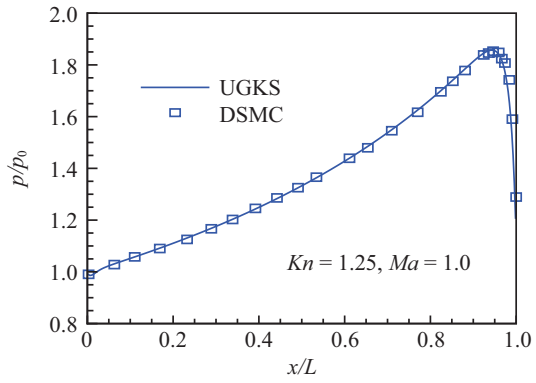

Fig. 4. Pressure distribution for $Kn = 1.25$ and $Ma = 1.0$.

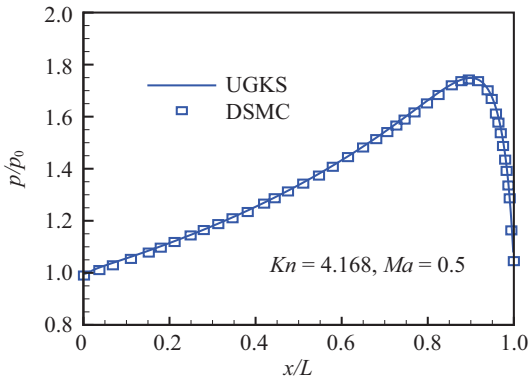

Fig. 5. Pressure distribution for $Kn = 4.168$ and $Ma = 0.5$.

If a heat spot is present on the disk, there will be a pressure bump in the pressure distribution, which has influence on the bearing force. Figure 6 shows comparison of the present pressure distribution with that of Myo et al.,[6] where the pressure bump is well captured by UGKS. The parameters are $\alpha = 0.01$ rad, $L = 5$ μm, $h_0 = 5$ nm, and $U = 30$ m/s with a 0.05 μm sized heat spot located 0.5 μm away from the exit on the disk. The gas is argon with $\mu \sim T^{0.81}$ in this case.

In order to fully understand the forcing effect on the air-bearing problem under different flow conditions, many cases with different Mach and Knudsen numbers are performed. The divergence of w_p and w_f could become quite obvious under some situations, due to the non-equilibrium of the gases. Figure 7 shows the distribution of the pressure to force (per unit area) ratio p/F for a given system. Although there exist big differences close to inlet and outlet, p/F is almost a constant in the bulk region, indicating a uniform non-equilibrium property in this region.

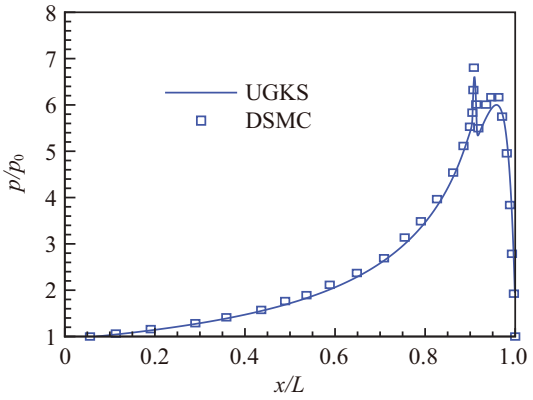

Fig. 6. Pressure distribution with heat spot present on disk.

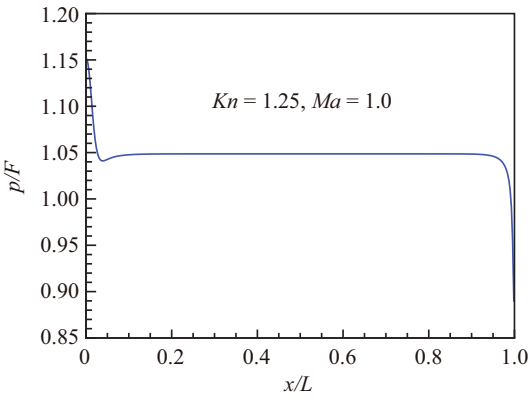

Fig. 7. Distribution of pressure to force ratio p/F.

The influence of Mach and Knudsen number on p/F, w_p, and w_f will be presented. In the simulations, the geometry is $L/h_0 = 100$, $\alpha = 0.01$ rad, the gas is hard-sphere argon and $Kn = 1.0$. Figure 8 shows the variation of p/F as a function of Mach number. And Fig. 9 shows the dependence of w_p and w_f on the Mach number individually. As Mach number increases, p/F increases at a higher rate, which indicates a stronger non-equilibrium effect. If w_p and w_f are examined individually, both w_p and w_f increase with Mach number when $Ma < 0.5$ and have almost the same values. At approximately $Ma = 0.5$, w_f reaches a maximum and the difference between w_f and w_p becomes obvious. For $Ma > 0.5$, w_f decreases with Mach number while w_p increases slowly. Mach number which indicates the speed of the slider is a driving force for the non-equilibrium transport in gases, but with the increasing flow speed the particle collisions with the wall will take a more effective way to reduce the non-equilibrium property. The behavior of w_f is a result of competition between these two effects.

The Knudsen number can be increased by keeping the ratio L/h_0, but reducing the system's size. In the following, the Mach number is a constant $Ma = 0.5$, and α, L/h_0 and gas properties are the same as used in the previous case. Figure 10 shows the variation of p/F as a function of Knudsen number. And Fig. 11 shows the dependence of w_p and w_f on the Knudsen number. As Kn increases, p/F increases and approaches to its free molecular limit. The pressure load w_p

exhibits a maximum value near $Kn = 2$, and changes slightly as Kn increases. But w_f decreases continuously with the increase of Kn.

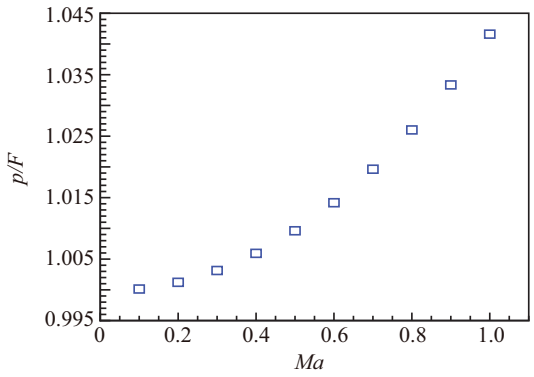

Fig. 8. p/F as a function of Mach number.

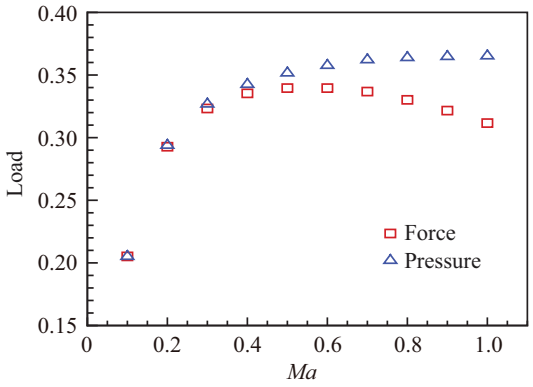

Fig. 9. w_p and w_f as a function of Mach number.

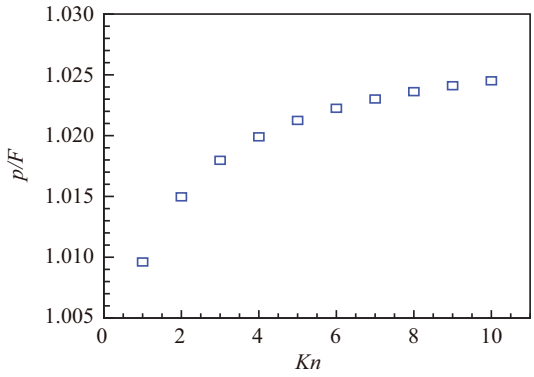

Fig. 10. p/F as a function of Knudsen number (reducing system's size).

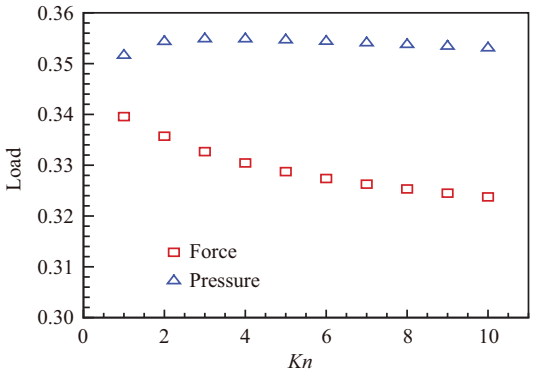

Fig. 11. w_p and w_f as a function of Knudsen number (reducing system's size).

The Knudsen number can also be increased by keeping α and L, but reducing h_0 alone. In this calculation, the gas is hard-sphere argon at ambient condition, the length is $L = 100\lambda$ and $\alpha = 0.01$ rad. As expected, p/F increases with Kn, as shown in Fig. 12. Different from previous one, the pressure load w_p and force load w_f have similar trend, but their difference gets smaller at high Knudsen number, as shown in Fig. 13.

In this letter, the UGKS method is briefly described and used to study the two-dimensional slider air bearing problem. The UGKS solutions are validated by comparison with the DSMC data, and good agreement has been obtained for both cases with or without a heat spot on the disk. The effect of Mach number and Knudsen number on the gas pressure load and force load on the slider per unit area is studied as well. The pressure to force ratio p/F increases as Mach number or Knudsen number increase. With a fixed Knudsen number, the force load w_f experiences a maximum value at a Mach number. And the force load w_f decreases when shrinking the system size and increases when reducing the minimum height between the slider and the disk.

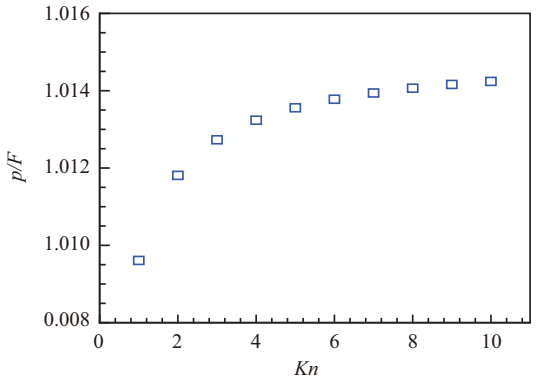

Fig. 12. p/F as a function of Knudsen number (reducing minimum height).

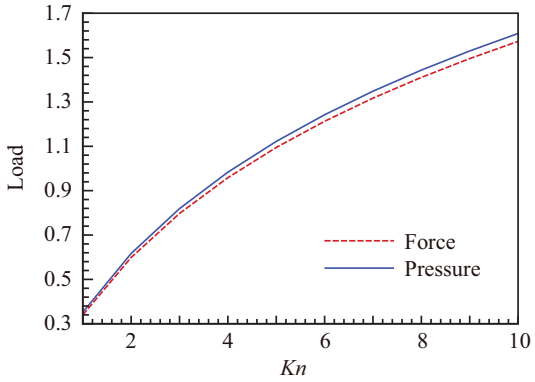

Fig. 13. w_p and w_f as a function of Knudsen number (reducing minimum height).

This work was supported by Hong Kong Research Grant Council (621011 and 620813) and HKUST (SRFI11SC05 and FSGRF13SC21).

1. S. Fukui, R. Kaneko. Analysis of ultra-thin gas film lubrication based on linearized Boltzmann equation: First report derivation of a generalized lubrication equation including thermal creep flow. *Journal of Tribology* **110**, 253–261 (1988).
2. S. Fukui, K. Yamane, H. Matsuoka. Novel laser-assisted micro levitation mechanism for magneto-optical recording. *IEEE Transactions on Magnetics* **37**, 1845–1848 (2001).
3. F. J. Alexander, A. L. Garcia, B. J. Alder. Direct simulation Monte Carlo for thin-film bearings. *Physics of Fluids* **6**, 3854–3860 (1994).
4. W. D. Huang, D. B. Bogy, A. L. Garcia. Three-dimensional direct simulation Monte Carlo method for slider air bearings. *Physics of Fluids* **9**, 1764–1769 (1997).
5. K. S. Myo, W. D. Zhou, S. K. Yu, et al. Direct Monte Carlo simulations of air bearing characteristics on patterned media. *IEEE Transactions on Magnetics* **47**, 2660–2663 (2011).
6. K. S. Myo, W. D. Zhou, S. K. Yu, et al. Direct Monte Carlo simulation of air bearing effects in heat-assisted magnetic recording. *Microsystem Technologies* **17**, 903–909 (2011).
7. K. S. Myo, W. D. Zhou, X. Y. Huang, et al. Slider posture effects on air bearing in a heat-assisted magnetic recording system. *Advances in Tribology* **2012**, 1–6 (2012).
8. K. Xu, J. C. Huang. A unified gas-kinetic scheme for continuum and rarefied flows. *Journal of Computational Physics* **229**, 7747–7764 (2010).
9. J. C. Huang, K. Xu, P. B. Yu. A unified gas-kinetic scheme for continuum and rarefied flows II: Multi-dimensional cases. *Communications in Computational Physics* **12**, 662–690 (2012).
10. J. C. Huang, K. Xu, P. B. Yu. A unified gas-kinetic scheme for continuum and rarefied flows III: Microflow simulations. *Communications in Computational Physics* **14**, 1147–1173 (2013).
11. S. Z. Chen, K. Xu, C. B. Lee, et al. A unified gas kinetic scheme with moving mesh and velocity space adaptation. *Journal of Computational Physics* **231**, 6643–6664 (2012).